ACS APPLIED ENERGY MATERIALS
Cite This: ACS Appl. Energy Mater. 2018, 1, 3323−3330
Article
www.acsaem.org

Bowl-Like and Apple-Like PdCu Hollow Microparticles with Mesoporous Nanoshells: Synthesis, Characterization, and Electrocatalytic Performance

Shao-Qing Liu,[†,‡] Yi-Tao Xu,[†] Jin-Qi Xie,[†] Guo-Qing Sheng,[†,‡] Yan-Wu Zhu,[‡] Xian-Zhu Fu,[*,†,§] Rong Sun,[*,†] and Ching-Ping Wong[†,∥,⊥]

[†]Shenzhen Institutes of Advanced Technology, Chinese Academy of Sciences, Shenzhen 518055, China
[‡]Institute of Nano Science and Technology, University of Science and Technology of China, Suzhou 215123, China
[§]College of Materials Science and Engineering, Shenzhen University, Shenzhen 518055, China
[∥]Department of Electronics Engineering, The Chinese University of Hong Kong, Hong Kong 999077, China
[⊥]School of Materials Science and Engineering, Georgia Institute of Technology, Atlanta, Georgia 30332, United States

Supporting Information

ABSTRACT: Novel bowl-like, apple-like, and spherical PdCu alloy hollow microparticles with mesoporous nanoshells are synthesized through a simple disproportionation reaction route using a spherical Cu_2O template with increasing H_2PdCl_4 ratio. The diameter of hollow particles is about 1 μm, and the thickness of mesoporous shells is about 50 nm. The obtained bowl-like PdCu alloy hollow microparticles with mesoporous nanoshells exhibit the highest electrocatalytic activity among the apple-like and spherical PdCu hollow microparticles and commercial Pd/C electrocatalysts toward methanol anodic oxidation for fuel cells. The remarkably excellent electrocatalytic performance of bowl-like PdCu alloy electrocatalysts might be attributed to the unique bowl-like hollow architecture with highly mesoporous nanoshells which are constructed by self-supported PdCu nanoparticles. The strategy presented here might help pave the way for the synthesis of novel nano-/microcomplex hollow materials with mesoporous nanoshells.

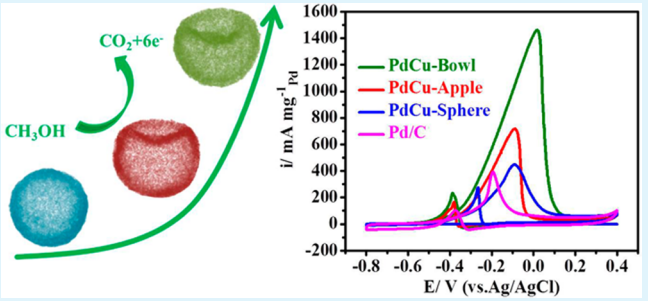

KEYWORDS: *hollow microparticle, mesoporous nanoshell, palladium copper alloy, direct methanol fuel cells, electrocatalysis*

1. INTRODUCTION

Hollow materials have higher surface area and lower density, which are highly desirable structural features for various applications, such as energy storage and conversion, catalysis, sensing, controlled delivery, etc.[1−8] Among various hollow materials, nanoalloy hollow materials are of great importance due to their excellent catalytic property.[9−12] Hollow alloy materials possess a high surface energy and abundant active sites due to the small-sized effects and numerous defects on surfaces. Their catalytic performances, including selectivity and stability, can be remarkably improved by alloying generally,[13−15] attributing to the reconfigurable electronic structures, which means the rearrangement of the valence electrons in the new potential fields formed by different elements' nuclei (instead of single element's) and related electrons.[16−18] Controlling the shapes, sizes, and compositions of hollow materials could further enhance the electrocatalytic activity. For example, various hollow structures including nanotubes,[19−21] hollow nanospheres,[22−27] and nanocubes[28−34] have been synthesized and exhibited outstanding electrocatalytic performance. Although a great variety of hollow alloy materials with different morphologies and structures have been synthesized, it is true that the rational design and synthesis of complex hollow alloy materials are still a great challenge. Nonetheless, the methods of synthesizing complex hollow structures are generally time-consuming and complicated, and the shell structure should be carefully controlled to improve the performance. Therefore, the rational design and synthesis of alloyed electrocatalysts with complex hollow structures are significant not only for fundamental studies, but also for catalytic applications.

Herein, we report a novel and simple strategy to synthesize unique bowl-like and apple-like PdCu alloy hollow microparticles with mesoporous nanoshells using Cu_2O microspheres as template. The ratio of H_2PdCl_4 and Cu_2O plays an important role in the morphology of PdCu alloy hollow microparticles in the preparation process. The bowl-like PdCu alloy hollow microparticles with mesoporous nanoshells exhibit

Received: March 30, 2018
Accepted: June 25, 2018
Published: June 25, 2018

DOI: 10.1021/acsaem.8b00523
ACS Appl. Energy Mater. 2018, 1, 3323−3330

remarkably superior electrocatalytic performance toward methanol oxidation compared to the apple-like and spherical PdCu alloy hollow microparticles and Pd/C commercial electrocatalysts.

2. EXPERIMENTAL SECTION

2.1. Materials. All reagents were of analytical purity and used without further purification. Cupric acetate ($Cu(CH_3COO)_2{\cdot}H_2O$, ≥99.5%), *N*,*N*-dimethylformamide (DMF), polyvinylpyrrolidone (PVP, K-30), glucose ($C_6H_{12}O_6$, ≥99.8%), palladium chloride ($PdCl_2$, ≥99.9%), sulfuric acid (H_2SO_4, ≥98%), hydrochloric acid (HCl, 37%), potassium hydroxide (KOH, ≥90%), and ethanol (C_2H_5OH, 99.7%) were purchased from Sinopharm Chemical Reagent Co., Ltd. (Shanghai, China). Commercial Pd/C (10.0%) was purchased from Aladdin Chemical Reagent Co, Ltd. The particle size of Pd is 10 nm. Deionized Milli-Q water (18 MΩ cm) was used for all experiments.

2.2. Materials Characterization. The morphologies and structures of as-synthesized samples were characterized by field-emission scanning electron microscopy (FE-SEM, FEI Nova Nano SEM 450) and high-resolution transmission electron microscopy (HRTEM, Tecnai G2 F20 FEI), respectively. The X-ray diffraction (XRD) patterns of as-prepared samples were recorded on a Rigaku D/Max 2500 X-ray diffractometer with Cu Kα radiation. The XPS data were gained by X-ray photoelectron spectroscopy (XPS) (ESCA Lab250 X-ray photoelectron spectrometer).

2.3. Synthesis of Monodisperse Cu_2O Spherical Microparticles. Typically, 1.6 g of $Cu(CH_3COO){\cdot}H_2O$, 0.6 g of PVP (K-30), and 1.52 g of glucose were dissolved in DMF (120 mL). After vigorous stirring for about 1.5 h, the solution was stirred for 10 min while the temperature was kept between 80 and 89 °C, and the color of the mixture became khaki. The final product was washed with alcohol and water three times and then dried in vacuum at 40 °C for 5 h.

2.4. Synthesis of PdCu/Cu_2O Precursors. A 10 mM H_2PdCl_4 aqueous solution was first prepared by completely dissolving 0.5 mmol of $PdCl_2$ in 20 mM HCl (50 mL) under ultrasonic treatment for 0.5 h. In a typical procedure, the synthesized Cu_2O particles (7.2 mg) and 0.55 g of PVP were redispersed in 20 mL of H_2O by sonication, and then, 10 mM H_2PdCl_4 (0.5 mL) was added. Then, the reaction was carried out at room temperature and ambient pressure for 20 min under magnetic stirring. The products were separated by centrifugation, washed with deionized water and ethanol three times, and dried in vacuum for overnight. The products were denoted as PdCu/Cu_2O-1. Another two types of PdCu/Cu_2O were prepared using different amounts of H_2PdCl_4. PdCu/Cu_2O synthesized with 1 and 3 mL of H_2PdCl_4 was denoted as PdCu/Cu_2O-2 and PdCu/Cu_2O-3, respectively.

2.5. Synthesis of Bowl-Like, Apple-Like, and Spherical PdCu Alloy Hollow Microparticles. In a typical procedure, a certain amount of PdCu/Cu_2O-1 precursors (10 mg) was dispersed into 20 mL of deionized water by sonication, and then, 18 mM H_2SO_4 (10 μL) was added. After reaction at room temperature for 5 min, the products were collected by centrifugation at 10 000 rpm for 5 min, washed by deionized water and ethanol three times, and dried in vacuum for 5 h to obtain bowl-like PdCu hollow microparticles with mesoporous nanoshells. The procedure for synthesis of apple-like and spherical PdCu hollow microparticles with mesoporous nanoshells was similar to that of the bowl-like PdCu hollow microparticles with mesoporous nanoshells, in which the difference was that a different PdCu/Cu_2O precursor was used (PdCu/Cu_2O-2 for preparation of apple-like PdCu alloy and PdCu/Cu_2O-3 for preparation of spherical PdCu alloy).

2.6. Synthesis of Pure Pd. A 10 mg portion of PdCu particles was dissolved in 50 mL of deionized water; 0.2 M (0.1 mL) HNO_3 was added, and the solution was stirred for 7 h.

2.7. Electrochemical Measurement. The electrochemical performance of catalysts was performed at room temperature using a three-electrode system consisting of a glassy carbon electrode (GCE, diameter, 5 mm; area, 0.196 cm^2), a platinum-plate counter electrode (1 cm × 1 cm), and a Ag/AgCl reference electrode at an electrochemical station (CHI 440C). The catalyst inks were prepared by dispersing the as-synthesized catalysts (4 mg) in a mixed solution containing 950 μL of ethanol and 50 μL of 0.1 wt % Nafion. The dispersion was sonicated for 0.5 h to form a homogeneous ink. Then, 10 μL of the dispersion was loaded onto the GCE dried at 40 °C. Prior to the test, the solution (1.0 M KOH + 1.0 M CH_3OH) was purged with pure Ar gas for 30 min. The electrochemically active surface area (ECSA) values of the as-prepared samples were determined by the charge involved in the hydrogen absorption/desorption region in 1 M H_2SO_4 solution in the cyclic voltammogram (CV). Methanol oxidation measurements were conducted in a solution containing 1.0 M KOH and 1.0 M CH_3OH at a sweep rate of 50 mV/s. Several activation scans were performed until the voltammogram curves were stable. Only the last voltammograms were collected for comparing the catalytic activity of the specified catalysts. The chronoamperometry tests were performed at −0.2 V for a period of 4000 s at room temperature. The chronopotentiometric curves were recorded in 1.0 M KOH and 1.0 M CH_3OH solution. CO stripping experiments were conducted in 0.5 M KOH. The electrolyte was first bubbled with 10% CO/N_2 while the potential of catalyst was held at −1.0 V for 30 min, during which CO monolayer adsorption was developed on the Pd surface. Unabsorbed CO was then expelled from the electrolyte by bubbling the solution with N_2 for 15 min. Then, CV cycles were performed immediately with an initial anodic sweep in the potential range from −0.9 to 0 V at 10 mV/s for at least two consecutive cycles.

3. RESULTS AND DISCUSSION

The synthesis process of bowl-like, apple-like, and spherical PdCu alloy hollow microparticles with mesoporous nanoshells is illustrated in Figure 1. First, the template of uniform

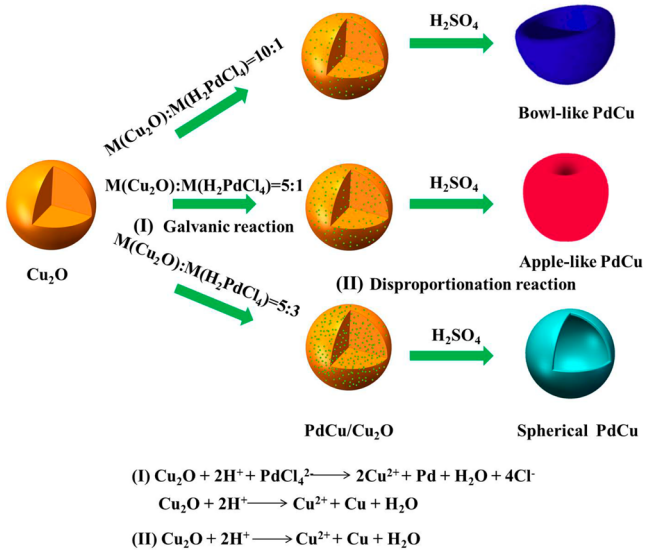

Figure 1. Schematic illustration of the formation process for bowl-like, apple-like, and spherical PdCu alloy hollow microparticles with mesoporous nanoshells.

spherical Cu_2O microparticles is synthesized by a solution-phase method according to the previous report.[35,36] The obtained Cu_2O microspheres are highly uniform with a mean size of 1 μm (Figure S1, Supporting Information). Second, the PdCu/Cu_2O microparticles are facilely achieved through the galvanic reaction between Cu_2O and metal ions in H_2PdCl_4 solution. The solution color changes from tan to dark green after the addition of H_2PdCl_4, indicating that the Pd^{2+} ions are

DOI: 10.1021/acsaem.8b00523
ACS Appl. Energy Mater. 2018, 1, 3323−3330

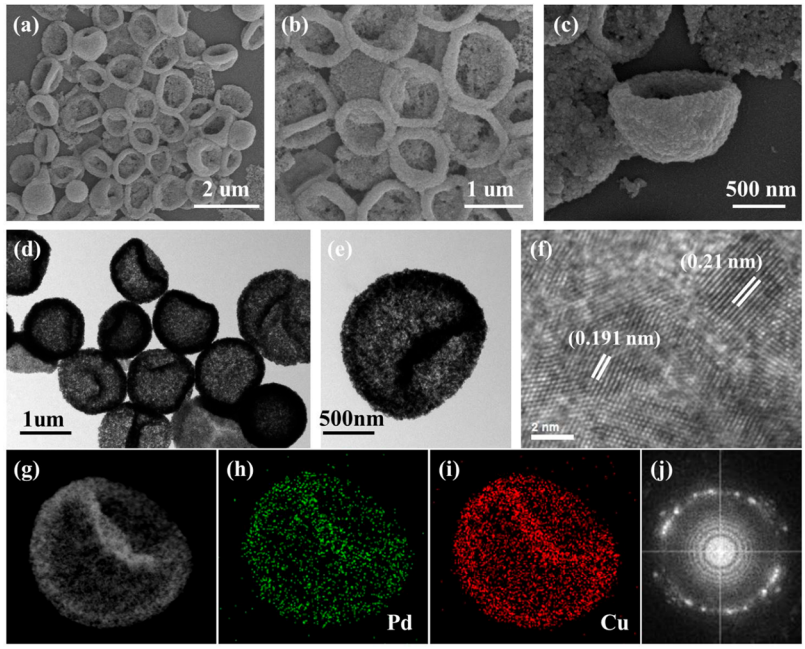

Figure 2. FE-SEM images of (a–e) bowl-like PdCu alloy hollow microparticles with mesoporous nanoshells. (f) HRTEM and (j) the corresponding FFT images of bowl-like PdCu alloy hollow microparticles with mesoporous nanoshells. (h, i) Elemental mapping images of individual bowl-like PdCu alloy hollow microparticles with mesoporous nanoshells shown in part g.

reduced quickly. During this fast galvanic reaction, the Cu forms on the surface of the Cu_2O template through the disproportionation reaction in the interfacial region between the aqueous solution of H_2PdCl_4 and Cu_2O (the detailed reactions are shown in the bottom of Figure 1). In the disproportionation reaction, the Cu(I) and $PdCl_4^{2-}$ could simultaneously react with H^+ to produce Cu and Pd, resulting in the formation of PdCu alloy particles.[37] Figures S2 and S3 (Supporting Information) show the heterogeneous PdCu/Cu_2O composite microspheres as indicated by step I in Figure 1. As depicted in Figure S2 and S3, it is obvious that the PdCu/Cu_2O particles still exhibit a spherical morphology. Moreover, the surface of PdCu/Cu_2O becomes smoother compared to that of the Cu_2O precursor. The energy-dispersive X-ray spectroscopy (EDS) result demonstrates that the sample contains Pd, Cu, and O elements (Figures S2 and S3, Supporting Information). As shown in Figure S2, the PdCu/Cu_2O particles obtained with 1 mL of H_2PdCl_4 are composed of Cu, O, and Pd with the atomic contents of 54%, 40%, and 6%, respectively. In addition, the PdCu/Cu_2O microparticles obtained with 0.5 mL of H_2PdCl_4 are composed of Cu, O, and Pd with the atomic contents of 62%, 35%, and 3%, respectively (Figure S3, Supporting Information). The HRTEM image in Figure S4a,b obviously shows the deposited PdCu alloy's intimate growth on the surface of the spherical Cu_2O support. The lattice spacing of 0.21 nm is between the Pd(111) plane (0.2265) and Cu(111) (0.2088 nm), implying the formation of PdCu alloy on the surface of Cu_2O. The elemental mapping results (Figure S4c–f) illustrate that the Pd element is uniformly distributed on the outer surface of a single Cu_2O spherical particle. Finally, the PdCu alloy is converted from these heterogeneous PdCu/Cu_2O particles through the disproportionation reaction between Cu_2O and H_2SO_4. The reaction processes could be formulated as shown in Reactions I and II (Figure 1). It should be noted that the molar ratio of Cu_2O and H_2PdCl_4 would influence the morphology of the final products. When the molar ratio of Cu_2O and H_2PdCl_4 is 10:1, the immaculate spherical particles are completely changed into deflated spheres with a bowl-like morphology. As the molar ratio of Cu_2O and H_2PdCl_4 is 5:1, PdCu alloy apple-like hollow microparticles are obtained. With the molar ratio of Cu_2O and H_2PdCl_4 decreased to 5:3, the as-prepared PdCu alloy is hollow microspheres.

As indicated in step II of Figure 1, when the mole ratio of Cu_2O and H_2PdCl_4 is 10:1, bowl-like PdCu alloy hollow microparticles with mesoporous nanoshells could be produced while keeping other parameters unaltered. Figure 2a–c shows that the spherical PdCu/Cu_2O microparticles are completely changed into bowl-like shape with a one-side open hole after disproportionation reaction between Cu_2O and H_2SO_4, resembling a bowl-like shape. The energy-dispersive X-ray (EDX) result displays that the bowl-like PdCu alloy hollow microparticles obtained with 0.5 mL of H_2PdCl_4 are composed of Pd and Cu with the atomic contents of 81% and 19%, respectively (Figure S5, Supporting Information). TEM images (Figure 2d,e) further reveal the well-defined cavity in the center of particles and hollow structure of one layer of mesoporous shell with a thickness of ≈50 nm. The magnified TEM image shown in Figure S9b further confirms that the PdCu alloy wall is porous and, moreover, consists of the interconnected homogeneous nanocrystals with a size of ≈20 nm. The energy-dispersive X-ray spectroscopy (EDX) elemental mapping result (Figure 2h,i) demonstrates the generally uniform distribution of Pd and Cu within the structure. The HRTEM image (Figure 2f) and the associated fast Fourier transform (FFT) in Figure 2j reveal that the PdCu alloys are polycrystalline. Two kinds of lattice spaces are observed; the 0.21 and 0.19 nm lattice space are smaller than those of the pure Pd (111) plane (0.227 nm) and Pd (100) (0.194 nm), but larger than pure Cu (111) (0.209 nm) and Cu (100) (0.181 nm), indicating the formation of PdCu alloy.

DOI: 10.1021/acsaem.8b00523
ACS Appl. Energy Mater. 2018, 1, 3323–3330

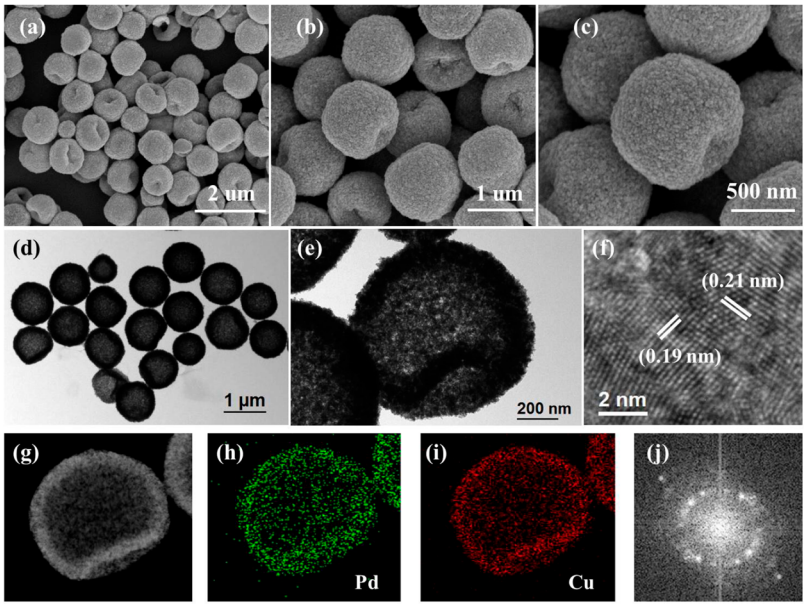

Figure 3. FE-SEM images of (a−e) apple-like PdCu alloy hollow microparticles with mesoporous nanoshells. (f) HRTEM and (j) the corresponding FFT images of apple-like PdCu alloy hollow microparticles with mesoporous nanoshells. (h, i) Elemental mapping images of individual apple-like PdCu alloy hollow microparticles with mesoporous nanoshells shown in part g.

A slight variation of the ratio of H_2PdCl_4 and Cu_2O would result in a different morphology of the PdCu alloy hollow microparticles. As indicated in step II of Figure 1, when the mole ratio of Cu_2O and H_2PdCl_4 is 5:1, apple-like PdCu alloy hollow microparticles with mesoporous nanoshells could be produced while keeping other parameters unaltered. As shown in Figure 3a−c, the PdCu microparticles are almost spherical with a one-side little cavity, resembling an apple shape. The particles are uniformly distributed with the average diameter of about 1 μm and relatively rough surface. As revealed by the TEM image, the transparency of the PdCu alloy microparticles confirms their hollow characteristics (Figure 3e). The shell of the nanocasting with a thickness of ≈95 nm exhibited an obviously mesoporous architecture (Figure S11, Supporting Information). The TEM image further reveals the well-defined cavity in the one side of particles. From Figure 3h,i, uniform distributions of Pd and Cu form an almost spherical morphology, which coincide with the mapping area of PdCu. According to the energy-dispersive X-ray (EDX) analysis, the apple-like PdCu alloy hollow microparticles obtained with 1 mL of H_2PdCl_4 were composed of Pd and Cu with the atomic contents of 82% and 18%, respectively (Figure S6, Supporting Information). The HRTEM images (Figure 3f) and the corresponding fast Fourier transform (FFT) (Figure 3j) results of apple-like PdCu microparticles are similar to those of the bowl-like PdCu hollow microparticles, suggesting the PdCu alloy phase.

The ratio of Pd^{2+} ions and the Cu_2O template plays an important role in the morphology of PdCu alloy hollow particles. To demonstrate the role of Pd, we conducted a comparative experiment with pure Cu_2O and H_2SO_4. As shown Figure S7, in absence of H_2PdCl_4, Cu particles could still be produced, but the spherical morphology is not retained at all; irregular Cu particles aggregate together. After the reaction of Cu_2O and H_2PdCl_4, the surface of Cu_2O would be covered with PdCu alloy, which could be seen from the TEM images of $PdCu/Cu_2O$ (Figure S4). Subsequently, as the disproportionation reaction is between $PdCu/Cu_2O$ and H_2SO_4, H_2SO_4 reacts with the internal Cu_2O, and the surface PdCu acts as a protective layer to prevent the collapse of spherical morphologies. As revealed by Figure S8, when the Pd atom content of $PdCu/Cu_2O$ increased to 19% (M_{Cu_2O}:$M_{H_2PdCl_4}$ = 5:3), a dense layer of PdCu alloy would be formed on the surface of Cu_2O. In the following step, when the H_2SO_4 reacted with inner Cu_2O, the spherical morphology could be preserved. Then, the PdCu shows spherical hollow morphology. When the Pd atom content decreases to 6%, the surface of the PdCu alloy becomes relatively sparse, which means that the capability of the PdCu protective layer become weaker, resulting in the collapse of spherical morphology to the apple shape. When the Pd atom content decrease to 3%, the spherical Cu_2O has a greater degree of collapse, forming bowl-shaped PdCu alloy microparticles. The ICP-MS results are shown in Table S1, which coincide with EDS results.

To further determine the crystallographic structure of these products, the X-ray diffraction (XRD) measurement was performed. As shown in Figure 4, all of the diffraction peaks in the Cu_2O spectra (black line) are perfectly assigned to the cubic Cu_2O (JCPDS 65-3288). The signal of Cu_2O in the $PdCu/Cu_2O$ spectra (red line) is weaker than that of the Cu_2O

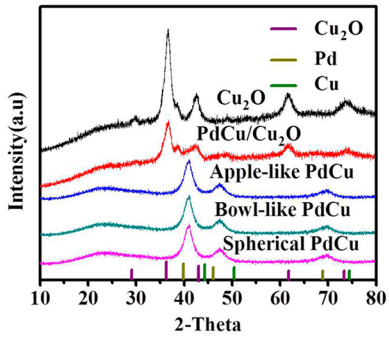

Figure 4. XRD patterns of Cu_2O microspheres, $PdCu/Cu_2O$ composite, and PdCu alloy hollow microparticles.

DOI: 10.1021/acsaem.8b00523
ACS Appl. Energy Mater. 2018, 1, 3323−3330

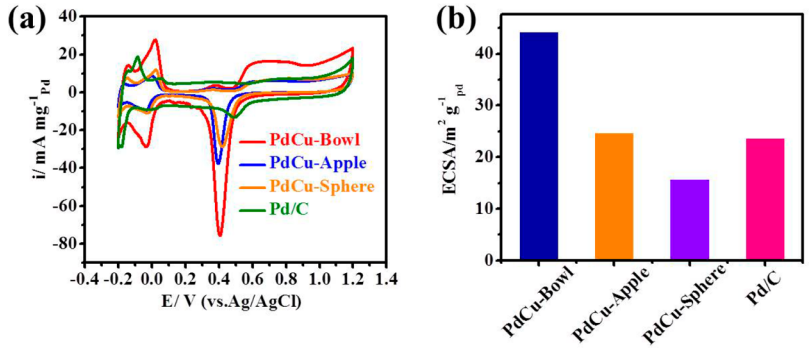

Figure 5. (a) Cyclic voltammetry curves of bowl-like, apple-like, and spherical PdCu hollow microparticles and commercial Pd/C electrocatalysts, which are recorded at room temperature with the scan rate of 50 mV/s in 0.5 M H_2SO_4 solution. (b) Electrochemically active surface area (ECSA).

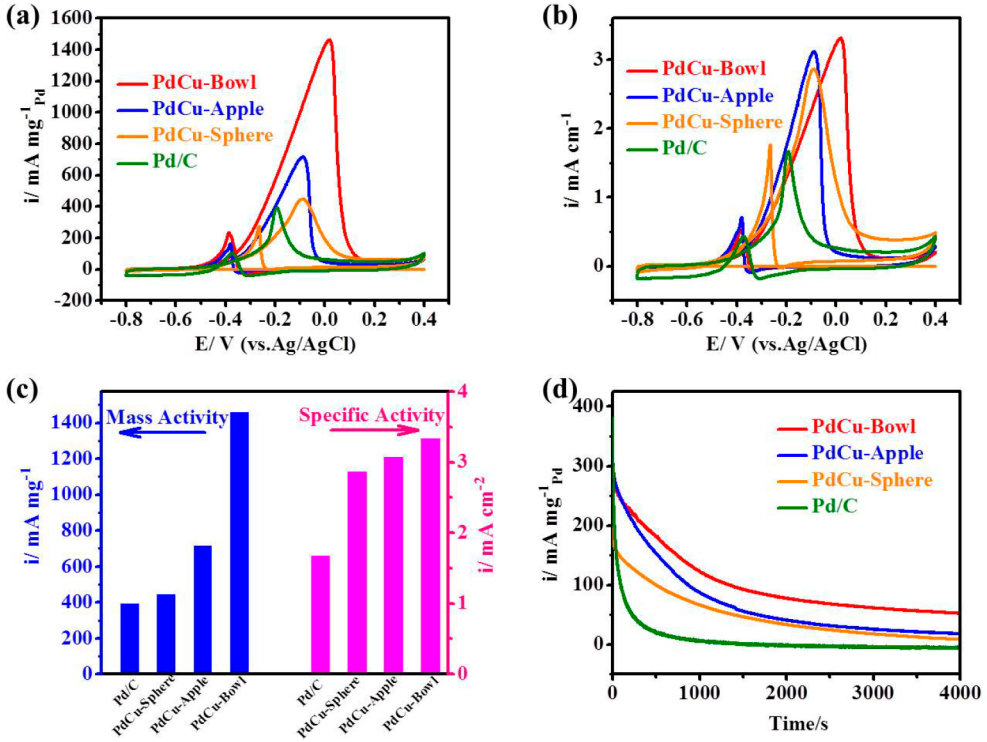

Figure 6. CV curves of bowl-like, apple-like, and spherical PdCu alloy hollow microparticles with mesoporous nanoshells and commercial Pd/C electrocatalysts recorded in a solution of 1 M KOH and 1 M CH_3OH: (a) CV curves normalized by mass activities, and (b) CV curves normalized by specific activities. (c) Mass activities and specific activities of the as-prepared hollow microparticles and commercial Pd/C. (d) Chronoamperometric curves for methanol oxidation.

template which might probably be because of the formation of the PdCu alloy in the surface of Cu_2O microparticles. The XRD pattern of bowl-like PdCu alloy hollow microparticles (green line) demonstrates that the (111), (200), and (220) crystalline plane diffraction peaks are located between pure fcc Pd (JCPDS 46-1043) and Cu (JCPDS 04-0836) crystal phases. The crystal size of bowl-like PdCu microparticles estimated from the full width at half-maximum of the (111) peak using the Scherrer equation indicates that the nanocrystals are (19 ± 0.3) nm in diameter, in good agreement with that measured from SEM and TEM images (Figure S9), which indicates that these PdCu alloy microparticles are constructed by nanocrystals. The X-ray diffraction (XRD) pattern of apple-like PdCu alloy hollow microparticles (blue line) is similar to that of bowl-like PdCu alloy hollow microparticles. The self-supported PdCu nanoparticles would not easily aggregate together. Neither characteristic peaks of Cu nor its oxides are detected, confirming the formation of pure PdCu alloy. The electronic structure of PdCu alloy hollow microparticles is further investigated by X-ray photoelectron spectroscopy. The results of the bowl-like PdCu alloy (Figure S10) are the same as those of the apple-like PdCu alloy. The Pd 3d spectrum exhibits peaks at 340.6 eV (Pd $3d_{3/2}$) and 335.2 eV (Pd $3d_{5/2}$), corresponding to Pd (0). The Cu 2p spectrum exhibits peaks at 931.9 eV (Cu $2p_{3/2}$) and 951.9 eV (Cu $2p_{1/2}$), and the auger kinetic energy shows 918.4 eV, indicative of elemental Cu(0).[38]

The electrocatalytic properties of as-prepared PdCu alloy hollow microparticles are evaluated in 0.5 M H_2SO_4 solution in comparison to commercial Pd/C, as shown in Figure 5. The ECSA of bowl-like PdCu alloy hollow microparticles is 44.15 m^2/g, which is about 1.8, 2.8, and 1.9 times that of the apple-like (24.6 m^2/g) and spherical PdCu alloy hollow microparticles (15.6 m^2/g) and commercial Pd/C nanosized

DOI: 10.1021/acsaem.8b00523
ACS Appl. Energy Mater. 2018, 1, 3323−3330

electrocatalysts (23.5 m^2/g), respectively. The high ECSA for PdCu hollow microparticles, especially bowl-like PdCu hollow microparticles, should result from the hollow architecture and mesoporous nanoshells fabricated by smaller PdCu nanoparticles.

The electrocatalytic performance of different morphologies of PdCu alloy hollow microparticles and commercial Pd/C electrocatalysts for methanol oxidation is evaluated by CV test in 1 M KOH + 1 M CH_3OH solution with a scanning rate of 50 mV/s, normalized by the mass of catalysts and estimated ECSA, respectively. Figure 6a,b is the mass activity and area activity converted, respectively. Figure 6c shows the area activity and mass activity of PdCu alloy hollow microparticles and commercial Pd/C electrocatalysts. The mass activity of the bowl-like PdCu alloy hollow microparticles is 1462 mA/mg, which is 2.04, 3.22, and 3.73 times those of the apple-like PdCu alloy hollow microparticles (716 mA/mg), PdCu alloy hollow spherical microparticles (453 mA/mg), and commercial Pd/C electrocatalysts (391 mA/mg). The specific activity of the bowl-like PdCu alloy hollow microparticles is 3.32 mA/cm^2, 1.07, 1.16, and 2 times, respectively, those of apple-like PdCu alloy (3.11 mA/cm^2) and PdCu alloy hollow spherical microparticles (2.85 mA/cm^2) and commercial Pd/C electrocatalysts (1.66 mA/cm^2). The bowl-like PdCu alloy hollow microparticles exhibit the highest catalytic activity among the PdCu alloy hollow microparticles. It is well-known that the activity of the catalyst is related to its morphology, size, structure, and composition. The bowl-like PdCu alloy hollow microparticles with mesoporous nanoshells exhibit remarkably superior electrocatalytic performance for methanol oxidation compared to the apple-like and spherical PdCu alloy hollow microparticles. This is because the thickness and density of the PdCu alloy particles are different. As shown in Figure S11, the shell thickness of bowl-like PdCu alloy particles is about 50 nm which is much thinner than those of apple-like (about 95 nm) and spherical PdCu alloy particles (about 110 nm). This means that methanol can easily access the internal surface of the bowl-like PdCu alloy. In this case, compared with that of the apple-like and spherical PdCu alloy, the inner surface of the bowl-like PdCu alloy could be effectively utilized for electrocatalysis. Then, the bowl-like PdCu alloy exhibits better electrocatalytic performance for the methanol oxidation reaction (MOR) in comparison with the apple-like and spherical PdCu alloy. Moreover, bowl-like PdCu also shows high mass activity and specific activity compared to other catalysts in the literature as listed in Table S2. In addition, the poison tolerance of electrocatalysts is also an important parameter for methanol oxidation. The ratio of forward oxidation peak (If) to the reverse oxidation peak (Ib) could assess the tolerance to carbonaceous species accumulation of electrocatalysts.[31,39,40] A high If/Ib ratio implies efficient removal of poisoning species on the surface of electrocatalysts. The If/Ib ratio of bowl-like PdCu alloy hollow microparticles is 6.2, which is 1.4 and 3.9 times those of the apple-like PdCu alloy hollow microparticles (4.3) and PdCu alloy hollow spherical microparticles (1.6). The enhanced electrocatalytic performance of the bowl-like PdCu alloy hollow microparticles might be attributed to the unique bowl-like hollow microarchitecture with highly mesoporous nanoshells fabricated by smaller nanosize PdCu alloy crystals and synergistic effect between Pd and Cu. To demonstrate the existence of synergistic effects, we compare the activity of pure Pd and Cu particles. As shown in Figure S12, pure Cu exhibits almost no activity toward the MOR. The mass activity of pure Pd is 44.8% lower than that of bowl-like PdCu, which highlights the advantage of the PdCu alloy in enhancing the electrocatalytic activity.

The electrochemical stability of PdCu alloy hollow microparticles with mesoporous nanoshells and commercial Pd/C electrocatalysts for methanol electro-oxidation is investigated by chronoamperometric experiments at a given potential of −0.2 V in the solution of 1 M KOH + 1 M CH_3OH (Figure 6d). The polarization current for the methanol electro-oxidation reaction shows a rapid decline in the initial period for all the samples, probably due to the formation of the intermediate species during the methanol oxidation reaction in alkaline media. After the 4000 s test, the oxidation current on the bowl-like PdCu alloy hollow microparticles is still 3 and 6.5 times higher than those of apple-like PdCu alloy hollow microparticles and PdCu alloy spherical hollow microparticles. To explain the stability improvements of the bimetallic catalysts, we performed the CO stripping test. As shown in Figure S13, the CO stripping peak potential for the bowl-like PdCu alloy is measured at −0.462 V, which is lower than those of apple-like PdCu alloy (−0.457 V), spherical PdCu alloy (−0.433 V), and commercial Pd/C (−0.383 V). The lower potential indicates that the Pd−CO bond becomes weaker on the alloyed samples. These Pd nanoparticles are more likely to be free from poisoning, ultimately leading to the observed excellent operation stability. The surface morphology of bowl-like PdCu alloy microparticles shows almost no change after the durability test, as shown in Figure S14, confirming the high structural stability of bowl-like PdCu. The excellent electrochemical stability of PdCu alloy hollow microparticles with mesoporous nanoshells might be due to the nanoparticles' self-supported hollow microstructure with high resistance for agglomeration and introduction of Cu-formed PdCu alloy to improve the poisoning tolerance.

The superior activity and stability of bowl-like PdCu alloy particles are mainly attributed to their unique morphology and composition.[41,42] The bowl-like morphology of the as-prepared PdCu allows methanol to easily access the internal surface, which provides a higher utilization of both their interior and exterior surfaces. The porous structure of the PdCu alloy particles could not only provide sufficient active catalytic sites but also allow the catalytic process to take place in a stable way, which inhibits the aggregation. The electronic structure of Pd could be changed by alloying Pd with Cu, which not only provides sufficient oxygenated species for methanol oxidation at a lower potential but also improves the poison tolerance of catalysts.[43,44]

4. CONCLUSIONS

A novel and efficient strategy is developed to synthesize bowl-like, apple-like, and spherical PdCu alloy hollow microparticles with mesoporous nanoshells using Cu_2O microspheres as a template. During the preparation, when the molar ratio of Cu_2O and H_2PdCl_4 is 10:1, the spherical particles are completely changed into deflated spheres with a bowl-like morphology. As the molar ratio of Cu_2O and H_2PdCl_4 is 5:1, PdCu alloy apple-like hollow microparticles are obtained. With the molar ratio of Cu_2O and H_2PdCl_4 decreased to 5:3, the as-prepared PdCu alloy is hollow microspheres. The PdCu alloy hollow microparticles, especially bowl-like PdCu hollow microparticles, demonstrate excellent electrocatalytic performance for methanol oxidation. The remarkable electrocatalytic

DOI: 10.1021/acsaem.8b00523
ACS Appl. Energy Mater. 2018, 1, 3323−3330

performance toward methanol oxidation reaction might be ascribed to the unique architecture of alloy nanoparticle self-supported hollow microstructures with highly porous features, which would bring benefits such as the enhanced charge transport and sufficient accessible active sites at both interior and exterior surfaces as well as the synergistic effect of the PdCu alloy.

■ ASSOCIATED CONTENT

Supporting Information

The Supporting Information is available free of charge on the ACS Publications website at DOI: 10.1021/acsaem.8b00523.

SEM images; TEM images; EDS spectroscopies; ICP-MS data of sample; XPS spectrum; CO stripping voltammetry measurements; and comparison of MOR activity with recently documented materials (PDF)

■ AUTHOR INFORMATION

Corresponding Authors

*E-mail: xz.fu@szu.edu.cn.

*E-mail: rong.sun@siat.ac.cn.

ORCID

Yan-Wu Zhu: 0000-0002-7505-1502

Xian-Zhu Fu: 0000-0003-1843-8927

Rong Sun: 0000-0001-9719-3563

Notes

The authors declare no competing financial interest.

■ ACKNOWLEDGMENTS

This work was financially supported by the National Natural Science Foundation of China (Grant 21203236), Guangdong Department of Science and Technology (Grant 2017A050501052), and Shenzhen research plan (Grant JCYJ20160229195455154).

■ REFERENCES

(1) Zhou, L.; Zhuang, Z.; Zhao, H.; Lin, M.; Zhao, D.; Mai, L. Intricate hollow structures: controlled synthesis and applications in energy storage and conversion. *Adv. Mater.* **2017**, *29*, 1602914.

(2) Kwon, T.; Hwang, H.; Sa, Y. J.; Park, J.; Baik, H.; Joo, S. H.; Lee, K. Cobalt Assisted Synthesis of IrCu Hollow Octahedral Nanocages as Highly Active Electrocatalysts toward Oxygen Evolution Reaction. *Adv. Funct. Mater.* **2017**, *27*, 1604688.

(3) Yu, L.; Wu, H. B.; Lou, X. W. D. Self-templated formation of hollow structures for electrochemical energy applications. *Acc. Chem. Res.* **2017**, *50*, 293−301.

(4) Hu, J.; Chen, M.; Fang, X.; Wu, L. Fabrication and application of inorganic hollow spheres. *Chem. Soc. Rev.* **2011**, *40*, 5472−5491.

(5) Liu, J.; Qiao, S. Z.; Budi Hartono, S.; Lu, G. Q. M. Monodisperse yolk−shell nanoparticles with a hierarchical porous structure for delivery vehicles and nanoreactors. *Angew. Chem.* **2010**, *122*, 5101−5105.

(6) Sun, Z.; Kim, J. H.; Zhao, Y.; Bijarbooneh, F.; Malgras, V.; Lee, Y.; Kang, Y.-M.; Dou, S. X. Rational design of 3D dendritic TiO_2 nanostructures with favorable architectures. *J. Am. Chem. Soc.* **2011**, *133*, 19314−19317.

(7) Sun, Y.; Mayers, B.; Xia, Y. Metal nanostructures with hollow interiors. *Adv. Mater.* **2003**, *15*, 641−646.

(8) Qi, J.; Lai, X.; Wang, J.; Tang, H.; Ren, H.; Yang, Y.; Jin, Q.; Zhang, L.; Yu, R.; Ma, G. Multi-shelled hollow micro-/nanostructures. *Chem. Soc. Rev.* **2015**, *44*, 6749−6773.

(9) Fang, H.; Yang, J.; Wen, M.; Wu, Q. Nanoalloy Materials for Chemical Catalysis. *Adv. Mater.* **2018**, *30*, 1705698.

(10) Wang, S.-B.; Zhu, W.; Ke, J.; Lin, M.; Zhang, Y.-W. Pd−Rh nanocrystals with tunable morphologies and compositions as efficient catalysts toward Suzuki cross-coupling reactions. *ACS Catal.* **2014**, *4*, 2298−2306.

(11) Chou, N. H.; Schaak, R. E. Shape-controlled conversion of β-Sn nanocrystals into intermetallic M-Sn (M= Fe, Co, Ni, Pd) nanocrystals. *J. Am. Chem. Soc.* **2007**, *129*, 7339−7345.

(12) Liu, S.; Zheng, X.; Song, L.; Liu, W.; Yao, T.; Sun, Z.; Lin, Y.; Wei, S. Partial-surface-passivation strategy for transition-metal-based copper−gold nanocage. *Chem. Commun.* **2016**, *52*, 6617−6620.

(13) Wang, D.; Li, Y. Bimetallic nanocrystals: liquid-phase synthesis and catalytic applications. *Adv. Mater.* **2011**, *23*, 1044−1060.

(14) Fang, H.; Chen, Y.; Wen, M.; Wu, Q.; Zhu, Q. SnNi nanoneedles assembled 3D radial nanostructure loaded with SnNiPt nanoparticles: Towards enhanced electrocatalysis performance for methanol oxidation. *Nano Res.* **2017**, *10*, 3929−3940.

(15) Wen, M.; Yang, D.; Wu, Q.-S.; Lu, R.-P.; Zhu, Y.-Z.; Zhang, F. Inducing synthesis of amorphous EuFePt nanorods and their comprehensive enhancement of magnetism, thermostability and photocatalysis. *Chem. Commun.* **2010**, *46*, 219−221.

(16) Zhang, J.; Sasaki, K.; Sutter, E.; Adzic, R. Stabilization of platinum oxygen-reduction electrocatalysts using gold clusters. *Science* **2007**, *315*, 220−222.

(17) Stamenkovic, V. R.; Fowler, B.; Mun, B. S.; Wang, G.; Ross, P. N.; Lucas, C. A.; Marković, N. M. Improved oxygen reduction activity on Pt_3Ni (111) via increased surface site availability. *Science* **2007**, *315*, 493−497.

(18) Stamenkovic, V. R.; Mun, B. S.; Arenz, M.; Mayrhofer, K. J.; Lucas, C. A.; Wang, G.; Ross, P. N.; Markovic, N. M. Trends in electrocatalysis on extended and nanoscale Pt-bimetallic alloy surfaces. *Nat. Mater.* **2007**, *6*, 241.

(19) Atkinson, R. W., III; St John, S.; Dyck, O.; Unocic, K. A.; Unocic, R. R.; Burke, C. S.; Cisco, J. W.; Rice, C. A.; Zawodzinski, T. A., Jr; Papandrew, A. B. Supportless, bismuth-modified palladium nanotubes with improved activity and stability for formic acid oxidation. *ACS Catal.* **2015**, *5*, 5154−5163.

(20) Wang, A. L.; He, X. J.; Lu, X. F.; Xu, H.; Tong, Y. X.; Li, G. R. Palladium−Cobalt Nanotube Arrays Supported on Carbon Fiber Cloth as High-Performance Flexible Electrocatalysts for Ethanol Oxidation. *Angew. Chem., Int. Ed.* **2015**, *54*, 3669−3673.

(21) Li, W.; Xiong, Y.; Wang, Z.; Bao, M.; Liu, J.; He, D.; Mu, S. Seed-mediated synthesis of large-diameter ternary TePtCo nanotubes for enhanced oxygen reduction reaction. *Appl. Catal., B* **2018**, *231*, 277−282.

(22) Li, F. M.; Zhai, Y. N.; Wu, Z. Q.; Li, S. N.; Lee, J. M. A Facile Self-Templated Approach for the Synthesis of Pt Hollow Nanospheres with Enhanced Electrocatalytic Activity. *Adv. Mater. Interfaces* **2016**, *3*, 1600563.

(23) Zhang, Y.; Li, J.; Rong, H.; Tong, X.; Wang, Z. Self-Template Synthesis of Ag−Pt Hollow Nanospheres as Electrocatalyst for Methanol Oxidation Reaction. *Langmuir* **2017**, *33*, 5991−5997.

(24) Wang, L.; Yamauchi, Y. Metallic nanocages: synthesis of bimetallic Pt−Pd hollow nanoparticles with dendritic shells by selective chemical etching. *J. Am. Chem. Soc.* **2013**, *135*, 16762−16765.

(25) Shi, H.; Liang, H.; Ming, F.; Wang, Z. Efficient Overall Water-Splitting Electrocatalysis Using Lepidocrocite VOOH Hollow Nanospheres. *Angew. Chem.* **2017**, *129*, 588−592.

(26) Liu, J.; Yang, Y.; Ni, B.; Li, H.; Wang, X. Fullerene-Like Nickel Oxysulfide Hollow Nanospheres as Bifunctional Electrocatalysts for Water Splitting. *Small* **2017**, *13*, 1602637.

(27) Zhu, J. W.; Zhou, H.; Zhang, C. T.; Zhang, J.; Mu, S. C. Dual active nitrogen doped hierarchical porous hollow carbon nanospheres as an oxygen reduction electrocatalyst for zinc-air batteries. *Nanoscale* **2017**, *9*, 13257−13263.

(28) Liu, D.; Xie, M.; Wang, C.; Liao, L.; Qiu, L.; Ma, J.; Huang, H.; Long, R.; Jiang, J.; Xiong, Y. Pd-Ag alloy hollow nanostructures with interatomic charge polarization for enhanced electrocatalytic formic acid oxidation. *Nano Res.* **2016**, *9*, 1590−1599.

(29) Huang, X.; Zhang, H.; Guo, C.; Zhou, Z.; Zheng, N. Simplifying the Creation of Hollow Metallic Nanostructures: One-Pot Synthesis of Hollow Palladium/Platinum Single-Crystalline Nanocubes. *Angew. Chem.* **2009**, *121*, 4902−4906.
(30) Hu, C.; Cheng, H.; Zhao, Y.; Hu, Y.; Liu, Y.; Dai, L.; Qu, L. Newly-Designed Complex Ternary Pt/PdCu Nanoboxes Anchored on Three-Dimensional Graphene Framework for Highly Efficient Ethanol Oxidation. *Adv. Mater.* **2012**, *24*, 5493−5498.
(31) Xia, B. Y.; Wu, H. B.; Wang, X.; Lou, X. W. One-pot synthesis of cubic PtCu3 nanocages with enhanced electrocatalytic activity for the methanol oxidation reaction. *J. Am. Chem. Soc.* **2012**, *134*, 13934−13937.
(32) Park, S.-K.; Kim, J. K.; Kang, Y. C. Metal−organic framework-derived CoSe $_2$/(NiCo)Se_2 box-in-box hollow nanocubes with enhanced electrochemical properties for sodium-ion storage and hydrogen evolution. *J. Mater. Chem. A* **2017**, *5*, 18823−18830.
(33) Wang, J. Y.; Mu, X.; Li, Y.; Xu, F.; Long, W.; Yang, J.; Bian, P.; Chen, J.; Ouyang, L.; Liu, H. Hollow PtPdRh Nanocubes with Enhanced Catalytic Activities for In Vivo Clearance of Radiation-Induced ROS via Surface-Mediated Bond Breaking. *Small* **2018**, *14*, 1703736.
(34) García, S.; Zhang, L.; Piburn, G. W.; Henkelman, G.; Humphrey, S. M. Microwave synthesis of classically immiscible rhodium−silver and rhodium−gold alloy nanoparticles: Highly active hydrogenation catalysts. *ACS Nano* **2014**, *8*, 11512−11521.
(35) Xu, Y.-T.; Guo, Y.; Li, C.; Zhou, X.-Y.; Tucker, M. C.; Fu, X.-Z.; Sun, R.; Wong, C.-P. Graphene oxide nano-sheets wrapped Cu_2O microspheres as improved performance anode materials for lithium ion batteries. *Nano Energy* **2015**, *11*, 38−47.
(36) Liu, S.-Q.; Wen, H.-R.; Zhu, Y.-W.; Fu, X.-Z.; Sun, R.; Wong, C.-P. Amorphous $Ni(OH)_2$ encounter with crystalline CuS in hollow spheres: A mesoporous nano-shelled heterostructure for hydrogen evolution electrocatalysis. *Nano Energy* **2018**, *44*, 7−14.
(37) Hong, F.; Sun, S.; You, H.; Yang, S.; Fang, J.; Guo, S.; Yang, Z.; Ding, B.; Song, X. Cu_2O template strategy for the synthesis of structure-definable noble metal alloy mesocages. *Cryst. Growth Des.* **2011**, *11*, 3694−3697.
(38) Zhao, X.; Dai, L.; Qin, Q.; Pei, F.; Hu, C.; Zheng, N. Self-Supported 3D PdCu Alloy Nanosheets as a Bifunctional Catalyst for Electrochemical Reforming of Ethanol. *Small* **2017**, *13*, 1602970.
(39) Huang, H.; Yang, S.; Vajtai, R.; Wang, X.; Ajayan, P. M. Pt-decorated 3D architectures built from graphene and graphitic carbon nitride nanosheets as efficient methanol oxidation catalysts. *Adv. Mater.* **2014**, *26*, 5160−5165.
(40) Sneed, B. T.; Young, A. P.; Jalalpoor, D.; Golden, M. C.; Mao, S.; Jiang, Y.; Wang, Y.; Tsung, C.-K. Shaped Pd−Ni−Pt core-sandwich-shell nanoparticles: influence of Ni sandwich layers on catalytic electrooxidations. *ACS Nano* **2014**, *8*, 7239−7250.
(41) Zhu, C.; Wen, D.; Oschatz, M.; Holzschuh, M.; Liu, W.; Herrmann, A. K.; Simon, F.; Kaskel, S.; Eychmuller, A. Kinetically Controlled Synthesis of PdNi Bimetallic Porous Nanostructures with Enhanced Electrocatalytic Activity. *Small* **2015**, *11*, 1430−1434.
(42) Liu, H. Q.; Adzic, R. R.; Wong, S. S. Multifunctional Ultrathin PdxCu1-x and Pt similar to PdxCu1-x One-Dimensional Nanowire Motifs for Various Small Molecule Oxidation Reactions. *ACS Appl. Mater. Interfaces* **2015**, *7*, 26145−26157.
(43) Chen, X. T.; Si, C. H.; Wang, Y.; Ding, Y.; Zhang, Z. H. Multicomponent platinum-free nanoporous Pd-based alloy as an active and methanol-tolerant electrocatalyst for the oxygen reduction reaction. *Nano Res.* **2016**, *9*, 1831−1843.
(44) Gilroy, K. D.; Ruditskiy, A.; Peng, H. C.; Qin, D.; Xia, Y. N. Bimetallic Nanocrystals: Syntheses, Properties, and Applications. *Chem. Rev.* **2016**, *116*, 10414−10472.

DOI: 10.1021/acsaem.8b00523
ACS Appl. Energy Mater. 2018, 1, 3323−3330